Thermal recuperative incineration of VOCs: CFD modelling and experimental validation

Sylvain Salvador, Jean-Michel Commandre, Yilmaz Kara

Thermal recuperative incineration of VOCs: CFD modelling and experimental validation

S. Salvador [a,*], J.-M. Commandré [a], Y. Kara [b]

[a] *Ecole des Mines d'Albi-Carmaux, Centre Energétique – Environnement, Laboratoire de Génie des Procédés des Solides Divisés UMR CNRS 2392, Campus Jarlard, Route de Teillet, 81013 Albi CT Cedex 09, France*

[b] *Gaz de France Research and Development Division, Industrial Utilisation Section, 361 Avenue du Président Wilson, 93211 Saint-Denis La Plaine Cedex, France*

Abstract

A numerical 2D model of a thermal recuperative incinerator (TRI) used to oxidise volatile organic compounds (VOCs) diluted in an air flow was developed to simulate the coupled equations for flow, heat transfer, mass transfer and progress of chemical reactions. The model was confronted with experimental values obtained on a highly instrumented half-industrial-scale pilot unit run under the same conditions. The model indicates that the flow inside the reactor is close to the ideal situation of a plug flow reactor. Nevertheless, a non-symmetric flow is retrieved despite the symmetrical arrangement of the combustion chamber. The model confirms that the most constraining phenomenon is the oxidation of CO. The formation of CO results of the combustion of the VOCs, and not from the combustion of the methane fed into the burner. The models demonstrated that the CO destruction reaction is controlled by the micro-mixing efficiency in a large part of the reactor, and not by the chemical kinetics of the reaction. This indicates the need for installing additional turbulence devices in order to enhance the turbulence level in a zone established from this modelling. The model establishes that thermal NO is formed in the flame zone of the burner, and is not due to VOC oxidation. These results together indicate that concentrating VOCs in an air flux prior to its treatment by a TRI will limit CO_2 emissions and NO emissions together.

Keywords: VOC; Recuperative incinerator; Modelling; Measurements; Pollutants

1. Introduction

Various industrial processes continuously generate air flows containing volatile organic compounds (VOCs). Given the toxicity of these compounds, and considering their impact on the greenhouse effect, it is necessary to treat these air flows before release into the atmosphere. One of the most commonly used techniques today is to oxidise them into CO_2 and H_2O using a thermal recuperative incinerator (TRI) [1,2]. The main advantages of this technique are the following:

- the small volume of the reactor in relation to the large air flows that can be treated;
- the possibility to treat air flows with low VOC contents, that cannot sustain self combustion;
- the tolerance of the process to changes in VOC concentration on a large scale.

The general principle of these reactors is recalled in Fig. 1. The air flux to be treated is preheated by a gas/gas heat exchanger prior to entering the combustion chamber (CC). A horizontal burner ramp (Fig. 3) is placed at the centre of the CC (Figs. 1 and 2). A small part of the air flow crosses the burner, enabling combustion of the natural gas (NG) that is fed into the burner, while the rest of the air flow crosses the air veins delimited by the burner ramp

* Corresponding author. Tel.: +33 5 6349 3127; fax: +33 5 6349 3243.
E-mail address: salvador@enstimac.fr (S. Salvador).

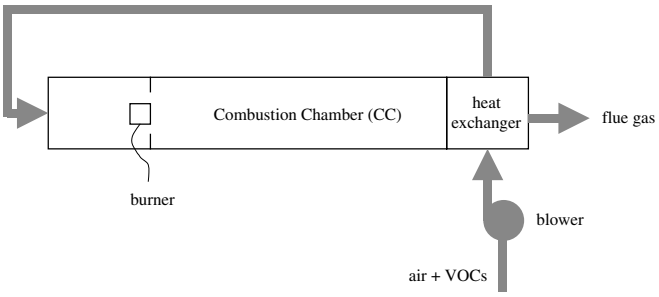

Fig. 1. General principle of a thermal recuperative incinerator.

and two diaphragms placed above and below the burner ramp. The thermal power of the burner is adjusted allowing the reaction temperature to reach typically 700–800 °C, and the length of the CC provides a residence time typically of between 0.5 and 1 s.

The design of these reactors, although they are used all over the world, remains essentially empirical. One reason for this is probably that numerous thermo-chemical and fluid-flow phenomena occur inside such reactors, and that their strong coupling make it impossible to perform simple calculations for their design.

The complexity of the process design also lies in the numerous demands constraining the process and in the multiple objectives that are fixed.

(i) The process needs to be secure; stable and continuous combustion must be ensured. This is achieved thanks to a "hard" high-temperature flame maintained downstream of the burner. The drawback is that this flame will generate thermal NO_X [3,4]; one objective will be to minimise these emissions.
(ii) Since the aim is to achieve minimum energy consumption and CO_2 emissions, the NG consumption of the burner needs to be minimised, which is equivalent to minimising the CC exit temperature. One can expect two drawbacks in lowering the temperature: the VOCs may not be oxidised, and CO – which is formed during the VOC oxidation process – may not be oxidised into CO_2. It has been established in previous work that the constraining phenomenon is CO emissions. At a low temperature, CO emissions exceed regulation limits while unburned hydrocarbon emissions are largely below regulations limits [3].

There are a priori a number of rules to follow during the design of a TRI for the above objectives to be reached:

(i) There should be no bypass in the flow of the polluted air through the combustion chamber. A preferential trajectory offering short residence time, low temperature or small turbulence intensity (see ii) would indeed result in a low oxidation of the VOCs and high CO concentration. In other words, a *plug flow* situation may be seen as ideal.
(ii) The intensity of the turbulence should be high enough to prevent limiting the chemical gas phase reactions by micro-mixing. Indeed, it has been established that the chemical reaction velocity can be limited either by chemical kinetics, or by micro-mixing of the fresh gases and of the products.

High turbulence levels are obtained in the combustion chamber through a number of artifices:

– the average velocity of the gases through the combustion chamber is high enough – typically several m s^{-1} – for the Reynolds number to be much larger than 2300, ensuring a turbulent flow;
– a restricted section for the passage of the air flow, called the *air veins*, is imposed by fitting the burner with two diaphragms. The flow downstream of each diaphragm is similar to step flow;
– the burner consists of a central NG injection ramp and two perforated plates – called *wings* – which are placed on both sides of this ramp, as shown in Figs. 2 and 3. Part of the air flow will cross the wings and ensure turbulent mixing of the NG with air flow. The two wings constitute an obstacle to the air flow, and will generate recirculation downstream, which also enhances turbulence.

There are a large number of parameters entering into the design of such reactors. The relative position of the burner

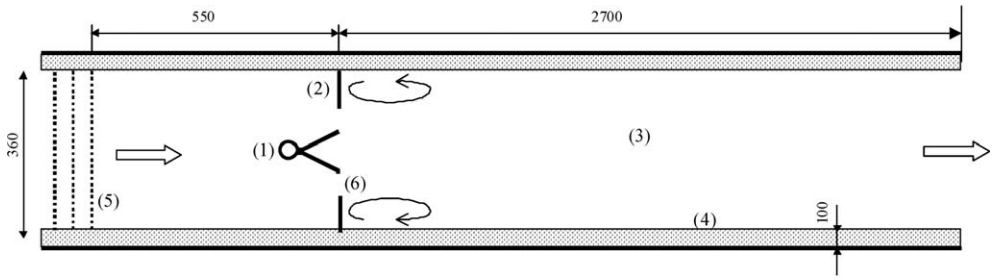

Fig. 2. General assembly of a VOC recuperative incinerator. (1) Burner; (2) diaphragms; (3) combustion chamber; (4) thermal insulation; (5) flow straightener; (6) air veins; (7) burner wings; (8) flame.

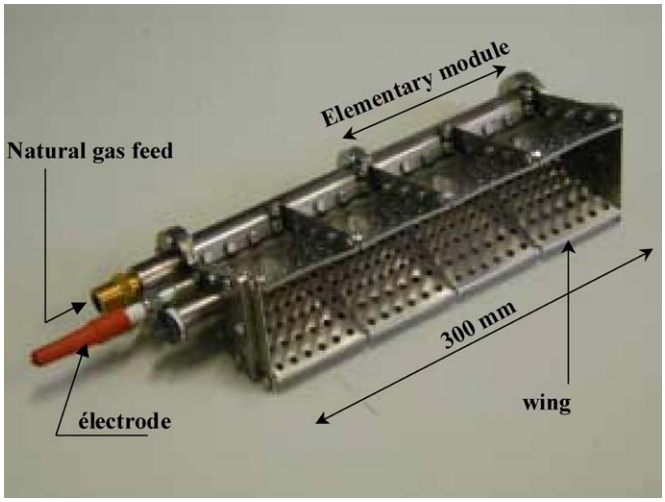

Fig. 3. Photograph of the burner from the pilot unit.

ramp and of the diaphragms can be varied. The height of the diaphragms is also a design parameter. A large number of design parameters can also be considered in the design of the burner itself. One can cite:

– the height and the angle of the wings;
  the number of rows of holes in the wings, the diameter of each hole, the shape of the holes and their arrangement;
– the injection velocity and the number of NG jets along the NG injection ramp;
– the fact that wings can be in contact with the NG injection ramp or can be fixed at a distance from it.

As a consequence, designing a TRI is a complicated task, and one can expect that modelling such reactors will be particularly helpful. In this paper, a numerical model describing the fluid flow, heat transfer and chemical reactions occurring inside the combustion chamber has been developed using the commercial Computational Fluid Dynamics (CFD) software, FLUENT. Confrontation with some experimental work has also been performed using a half-industrial-scale pilot unit described in detail elsewhere [3,5], and confirms the main conclusions of this work. An understanding of the fluid flow inside the reactor is achieved; an unanticipated asymmetry of the flow is observed. The sources for the main pollutants – NO, CO, unburned HC – are identified. This modelling was at the origin of two previously published technological improvements [5,6] that achieved a reduction in the NO emissions and NG consumption of the process.

2. Selection of the configuration for experimental work and modelling

There were two types of constraints in the choice of the configuration: constraints regarding the experimental work and numerical constraints.

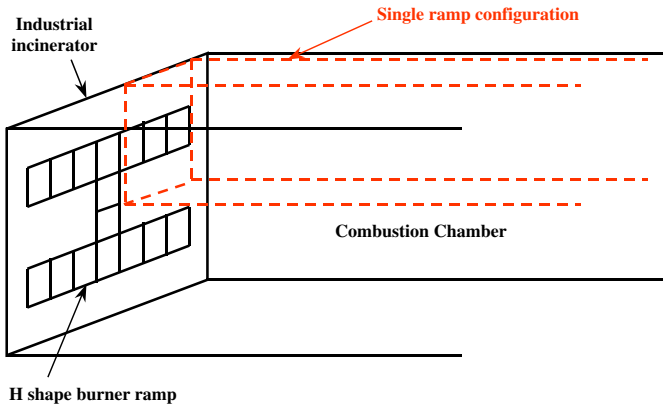

Fig. 4. Arrangement of an H-shape assembly of burner ramps in a large capacity recuperative incinerator – in dotted line, arrangement for a single ramp configuration.

In industrial scale TRI, the same burner design is always used when attempting to obtain large treatment capacities. This is achieved using quite complex H or I shape assembly of burner ramps, in order to cover a large section of reactor in a uniform way. These ramps consist of elementary burner modules placed side by side as illustrated in Fig. 4 in the case of H-shape assembly. Taking a simplified approach, one can assume that the flow pattern for such an assembly can be understood from the study of a single ramp, as illustrated by dotted lines in the figure. This configuration was adopted for the design of a half-industrial-scale pilot incinerator [3,5,6] and for the modelling work here presented. A vertical cross-section of a horizontal single ramp TRI is represented in Fig. 2, which also describes the pilot unit and gives a general view of the modelled geometry.

As regards the generally long length used for the burner ramps, 2D modelling was adopted. The validity of this choice is open to question: since the air flow through the two air veins can be seen as jets, the question of the stability of these jets is raised. This point will be discussed in more depth later in this paper.

3. Description of the model

3.1. Detailed geometry and mesh

The modelled geometry is described in detail in Figs. 2 and 5 and in Table 1. It corresponds with the configuration of the pilot unit used later to validate modelling. The description in this 2D model of the rows of holes in the burner wings was made as follows. Each row of holes in the burner wings was described by a slot; the aperture of each slot is calculated to offer the same free section as the holes in a given row. The exact geometry for the 10 slots is given here in Table 1 through the coordinates of the bottom left and of the top right limit of each slot. The same approach was adopted to describe the NG injection. This is equivalent to maintaining in the model the same average jet velocity as in the real burner.

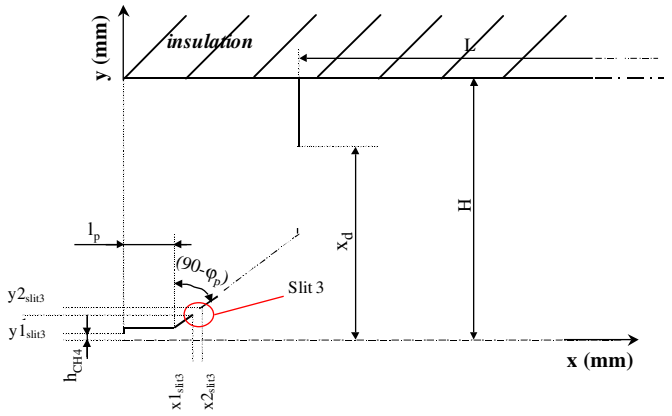

Fig. 5. Arrangement of the burner and of the combustion chamber.

Table 1
Geometrical arrangement of the burner and combustion chamber

	x (mm)		y (mm)	
Slit 1	4.957	5.043	0.3	0.3
Slit 2	6.957	7.043	0.3	0.3
Slit 3	13.823	14.177	3.911	4.061
Slit 4	20.585	21.215	6.781	7.048
Slit 5	28.385	29.015	10.092	10.359
Slit 6	37.446	38.154	13.938	14.238
Slit 7	48.596	49.304	18.671	18.971
Slit 8	59.696	60.404	23.382	23.683
Slit 9	72.428	73.372	28.787	29.188
Slit 10	85.328	86.272	34.263	34.663

Angle of the wings	$\varphi_p = 23°$
Length before bending	$l_p = 10.5$ mm
Methane feed slit half height	$h_{CH_4} = 0.08$ mm
Half height of the combustion chamber	$H = 180$ mm
Length of the combustion chamber	$L = 2700$ mm
Position of the diaphragm	$x_d = 93.4$ mm

Only one-half of the symmetrical geometry was simulated. The mesh was of the unstructured type in a zone close to the burner and structured downstream, as illustrated in Fig. 6. The total number of meshes was approximately 42,500. A preliminary study of the impact of the solution of the number of meshes indicated that beyond 40,000 meshes, the computed solution did not depend on the meshes any more.

3.2. Boundary conditions

The modelled configuration – which was similar to the configuration on the pilot unit during the experimental validation tests – corresponds with the optimal configuration of the TRI. This was determined precisely using the *experimental technique* [3,7]. Since the aim of the work is to improve the design of TRIs, it is logical to analyse and understand the best actual situation.

A flow of 470 $m^3\,s^{-1}$ at STP of air charged with 6.9 g_{COV}/m^3 at STP is fed in. This concentration of VOC, which is equivalent to 35% of the concentration for combustion self support, is an average of typical values operating in a TRI (2–20 g_{COV}/m^3 at STP). The conditions for the polluted air at the entrance of the chamber ($x = 0$) are given in Table 2. The intensity of the turbulence of 6.84% was estimated from measurements on the pilot unit using hot wire anemometry (see below). The VOC compound retained here is ethyl acetate, $C_4H_8O_2$, and was present in a mass fraction of 1.765×10^{-3}. The conditions for the inlet of NG are also reported in Table 2; 6.21 $m^3\,s^{-1}$ at STP are fed in at room temperature leading to an average injection velocity of 36.84 m s^{-1}. Since no measurement was possible in the NG feed, the value of 10% for the turbulence intensity was adopted as a standard value for flows in pipes [3,8,9].

In order to describe the heat loss through the walls of the CC as estimated from the temperature of the outside walls, an equivalent thermal flux of 330 W/m^2 was adopted as the boundary condition inside. The pressure at the exit of the CC was fixed at atmospheric pressure.

3.3. Flow and heat transfer

The balance equations used were the standard ones in FLUENT 6; they will not be restated here. Mass balance, momentum balance, enthalpy balance and a species balance for each gas species were solved. Reynolds Average Navier-Stokes (RANS) formulation was used. The fluid was assumed to be Newtonian, and to follow the perfect gas law. The $k-\varepsilon$ were used as the closure equations; standard values for the constants were adopted.

Radiation heat transfer was not taken into account in the simulation presented. The reason for this is that the validity of the pre-programmed models cannot easily be

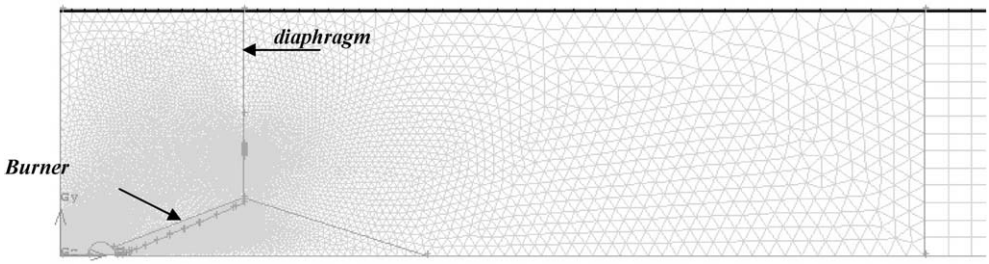

Fig. 6. Illustration of the 2D mesh.

Table 2
Boundary conditions

Air feed velocity (flow rate of 468 m^3/h STP)	$V_{air} = 2.552\ m\ s^{-1}$ (at 376 °C)
Air feed temperature	$T_{air} = 376$ °C
Air feed turbulence intensity	$I_t = 6.84\%$
Mass fraction of O_2	$x_{O_2} = 0.233$
Mass fraction of $C_4H_8O_2$ in air (6.9 g_{COV}/m^3 STP)	$x_{C_4H_8O_2} = 1765 \times 10^6$
Methane feed velocity (flow rate of 6.21 m^3/h STP)	$V_{CH_4} = 36.84\ m\ s^{-1}$
Methane feed temperature	$T_{CH_4} = 20$ °C
Methane feed turbulence intensity	$I_t = 10\%$
Heat flux at the walls	$\Phi_p = -330\ W/m^2$

estimated. Taking radiation into account using the models of the type P^n had some impact on the solution, changing the temperature close to the walls by 50 °C, but did not affect the conclusions reported in the sequel of the paper.

3.4. Chemical reactions

The chemical reactions occurring in the CC were described using the following simple reaction scheme including four non-reversible reactions. Hautman et al. [10] describe in their work the construction procedure for such reduced schemes. It was not possible to run a detailed reaction scheme with such a complex geometry in affordable computation time.

$$CH_4 + \frac{3}{2}O_2 \rightarrow CO + 2H_2O \quad (1)$$

$$C_4H_8O_2 + 3O_2 \rightarrow 4CO + 4H_2O \quad (2)$$

$$CO + \frac{1}{2}O_2 \rightarrow CO_2 \quad (3)$$

$$CO_2 \rightarrow CO + \frac{1}{2}O_2 \quad (4)$$

NG is composed of more than 95% methane. Methane is here supposed to oxidize into CO and H_2O following Eq. (1). The kinetic parameters for this reaction were obtained from [11].

The VOC ethyl acetate is also assumed to be first oxidised into CO and H_2O. Since no kinetic parameters for this reaction could be found in the literature, for this reaction we adopted the activation energy found by [8] for butane (C_4H_{10}). The pre-exponential factor was set in order to retrieve with the model the fraction of unburned hydrocarbon experimentally measured on the pilot unit, in the same conditions.

The oxidation of CO into CO_2 was described from Eq. (3); the kinetic parameters for this reaction can be found from [11,12]. This reaction is reversible. Nevertheless, describing it as a reversible reaction in the CFD code leads to difficulties [13,14], and it is standard practice to describe the equilibrium using an additional reaction, here Eq. (4). The pre-exponential factor for this reaction was here set in order to recover the CO fractions at the exit of the CC measured in the pilot unit.

Summarising this, the expressions for the reaction rate of the four equations are given by the following equations where the values for the constants can be found in Table 3.

$$-\frac{d[CH_4]}{dt} = A_{0_1} T^{\beta_1} \exp\left(\frac{-Ea_1}{RT}\right)[CH_4]^{a_1}[O_2]^{b_1} \quad (5)$$

$$-\frac{d[C_4H_8O_2]}{dt} = A_{0_2} T^{\beta_2} \exp\left(\frac{-Ea_2}{RT}\right)[C_4H_8O_2]^{a_2}[O_2]^{b_2} \quad (6)$$

$$-\frac{d[CO]}{dt} = A_{0_3} T^{\beta_3} \exp\left(\frac{-Ea_3}{RT}\right)[CO]^{a_3}[O_2]^{b_3}[H_2O]^{c_3} \quad (7)$$

$$-\frac{d[CO_2]}{dt} = A_{0_1} T^{\beta_4} \exp\left(\frac{-Ea_4}{RT}\right)[CO_2]^{a_4} \quad (8)$$

Since the reactions involving NO do not affect the balance equations, the fraction of NO is computed as a post treatment, for sake of computation rapidity. The NO formation is here computed from the extended Zeldovich mechanism for thermal NO [8], completed with a partial equilibrium approach for the calculation of O radicals [9,15].

$$O + N_2 \overset{k_1}{\leftrightarrow} N + NO \quad (9)$$

$$N + O_2 \overset{k_2}{\leftrightarrow} O + NO \quad (10)$$

$$N + OH \overset{k_3}{\leftrightarrow} H + NO \quad (11)$$

The global production of NO is expressed from

$$\frac{d[NO]}{dt} = k_{+1}[O][N_2] + k_{+2}[N][O_2] + k_{+3}[N][OH] - k_{-1}[NO][N] - k_{-2}[NO][O] - k_{-3}[NO][H] \quad (12)$$

with

$$k_{+1} = 1.8 \times 10^8 \exp\left(\frac{-38370}{T}\right)\ m^3\ mol^{-1}\ s^{-1} \quad (13)$$

$$k_{-1} = 3.8 \times 10^7 \exp\left(\frac{-425}{T}\right)\ m^3\ mol^{-1}\ s^{-1} \quad (14)$$

$$k_{+2} = 1.8 \times 10^4 T \exp\left(\frac{-4680}{T}\right)\ m^3\ mol^{-1}\ s^{-1} \quad (15)$$

$$k_{-2} = 3.8 \times 10^3 T \exp\left(\frac{-20820}{T}\right)\ m^3\ mol^{-1}\ s^{-1} \quad (16)$$

$$k_{+3} = 7.1 \times 10^7 \exp\left(\frac{-450}{T}\right)\ m^3\ mol^{-1}\ s^{-1} \quad (17)$$

$$k_{-3} = 1.7 \times 10^8 \exp\left(\frac{-24560}{T}\right)\ m^3\ mol^{-1}\ s^{-1} \quad (18)$$

Table 3
Summary of the kinetic parameters

Reaction	Source	A_0 (s^{-1})	Ea (J/kmol)	a	b	c
5	Dryer et al. [40]	5012×10^{11}	2000×10^8	0.70	0.80	
6		2000×10^7	1256×10^8	0.15	1.60	
7	Westbrook et al. [155]	2239×10^{12}	1700×10^8	1.00	0.25	0.50
8		7500×10^8	1700×10^8	1.00		

In these expressions, k_{+1}, k_{+2} and k_{+3} are the kinetic constant for the direct reactions (9)–(11), when k_{-1}, k_{-2} and k_{-3} characterize the reverse reactions.

The concentration in O radicals can be expressed from Warnatz et al. [16]

$$[O] = 36.64T^{1/2}[O_2]^{1/2} \exp\left(\frac{-27123}{T}\right) \text{ mol m}^{-3} \quad (19)$$

3.5. Calculation of chemical reaction rates

A particularly important aspect of the modelling is the need to take into account the fact that a chemical reaction can be controlled either by chemical reaction kinetics or by micro-mixing efficiency. The limiting phenomenon can be different from one place inside a reactor to another. It essentially depends on the species concentrations, the local temperature and kinetic constants as far as reaction kinetics is concerned, and on the kinetic energy and its dissipation rate as far as micro-mixing is concerned.

One of the strategies of the FLUENT software is the so-called "*finite rate-eddy dissipation*" model. In this approach, the software computes, at any location in the volume:

– a chemical reaction rate, based on the Arrhenius approach, assuming perfect mixing of the reactants and product species;

– a micro-mixing reaction rate, based on the turbulence of the flow, and assuming infinitely rapid chemical kinetics. This theory was first proposed by Magnussen et al. [17].

The software then adopts the smaller of the two reaction rates, since it is controlling the reaction progress.

Finally all equations are solved at steady state using a finite volume formulation. The SIMPLE algorithm is used to describe the relation between the velocity and the pressure. The under-relaxation factors are adjusted for a numerically stable and rapid convergence. The equations are solved at the second order to limit errors generated by numerical diffusion.

4. Results and interpretation

All the following plots, unless mentioned, are constructed using the calculated values and by drawing the symmetrical field, in order to facilitate reading.

4.1. Flow pattern

The resulting fluid velocity inside the CC can be described from Fig. 7 where we have plotted the average total velocity both for the whole CC and in detail for the burner zone; the recirculations that appear are represented by bold arrows. This representation was preferred to

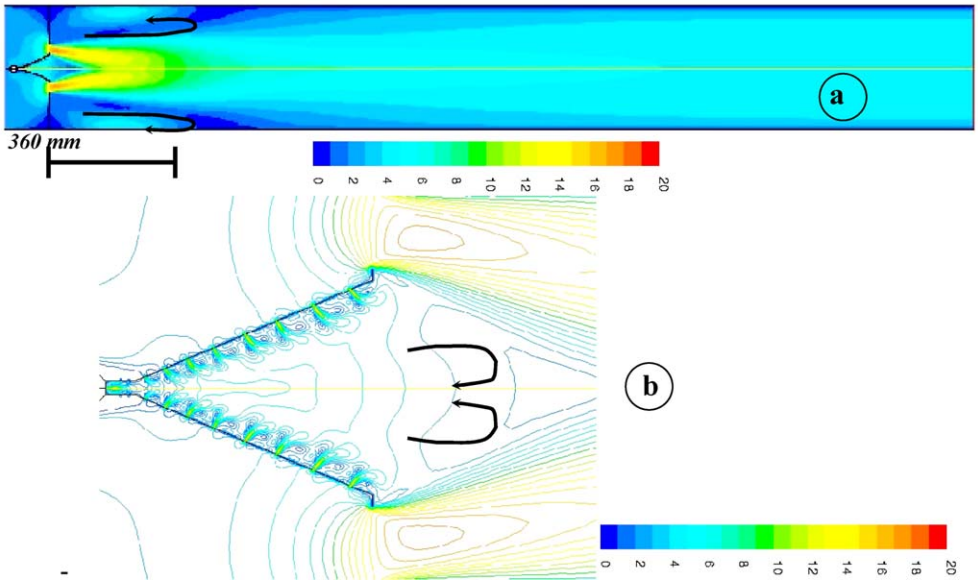

Fig. 7. Distribution of the average total velocity (m s^{-1}) inside the combustion chamber (a) and inside the burner (b).

arrows; the very low velocities in the recirculations made such a graph difficult to read. Two plane jets logically appear in the air veins, in which the velocity reaches 20 m s^{-1}. The zone downstream of the diaphragms and of the burner is characterised by two pairs of recirculations. Large dimension vortices are stabilised in the zone close to the walls, while small counter-rotating vortices appear downstream of each burner wing. Approximately 500 mm downstream of the diaphragms, which, thanks to the recirculations, remains a short distance, the velocity field is uniform. The velocity tends towards zero only in a zone very close to the walls; this is the result of the high Reynolds number flow in the CC. Indeed, the average exit velocity is 4.4 m s^{-1}, corresponding to a Reynolds number higher than 57,000. Consequently, most of the CC behaves as a plug-flow highly turbulent reactor with regard to the flow velocity.

4.2. Turbulence intensity

The intensity of the turbulence is represented in Fig. 8. The intensity can reach values as high as 400% in the air veins, and remains above 200% in a large zone up to $x = 500$ mm. Again, downstream of this zone, the intensity of the turbulence is quite uniform, at values in the range 200% down to 59% at the exit of the CC.

4.3. Temperature levels

The temperature field shown in Fig. 9, indicates that the uniformity of the temperature is not as good as one might expect. A zone centred on the symmetry plane is heated to temperatures higher than 1100 K along more than one-third of the length of the CC; in this zone, the temperature can reach 2300 K (see burner detail). The zone covered by the two large recirculations remains at a low temperature, in the range 700–800 K; chemical reactions are not active in this zone. The average exit temperature is 762 °C.

Measurements were taken inside the pilot unit running in conditions similar to that of the model. Small (125 μm) diameter nude-wire type R thermocouples were used; a correction for radiative heat exchange with the walls was operated on the raw values registered to calculate the gas temperature. Results are reported in Fig. 10, together with the results of the model (already presented under another form). At $x = 140$ mm, the model satisfactorily describes the temperature profile, retrieving the peak at more than 1500 K. The diminishing of the central peak along the CC is also observed experimentally. One can note the asymmetry in the temperature field between the top half and the bottom half of the CC. This questionable result is discussed in detail further in this paper.

4.4. Chemical species

The two fuels fed to the CC, i.e., the NG and the vinyl acetate, are almost absent at the exit of the CC: their average concentration is less than 2 ppm. Their cracking into CO is very rapid and efficient. This is in concordance with previous experimental work that demonstrated that non-chlorinated VOCs were destroyed with an efficiency of more than 99.999% as soon as the exit temperature was higher than 730 °C [3,7]. CH_4 is rapidly converted into CO in the flame zone of the burner (from examination of CH_4 concentration field, not shown here).

The CO fraction at the exit of the CC, on the other hand, is high at 53 ppm. As reported before, CO oxidation is the more constraining objective, and special attention will be paid to its formation and destruction.

As far as experimental gas species concentrations are concerned, the work consisted of on-line sampling and analysis at different locations. A water-cooled probe with

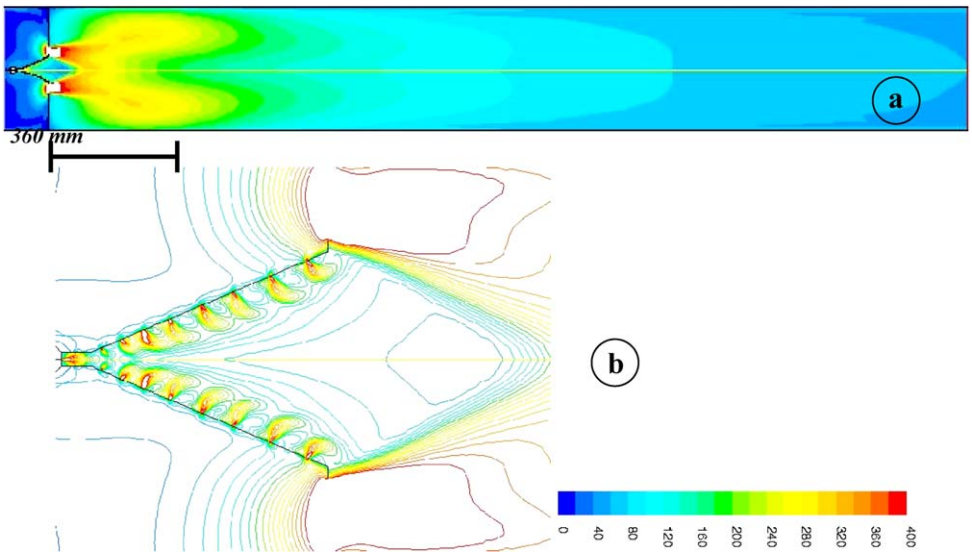

Fig. 8. Distribution of the turbulence intensity (%) inside the combustion chamber (a) and inside the burner (b).

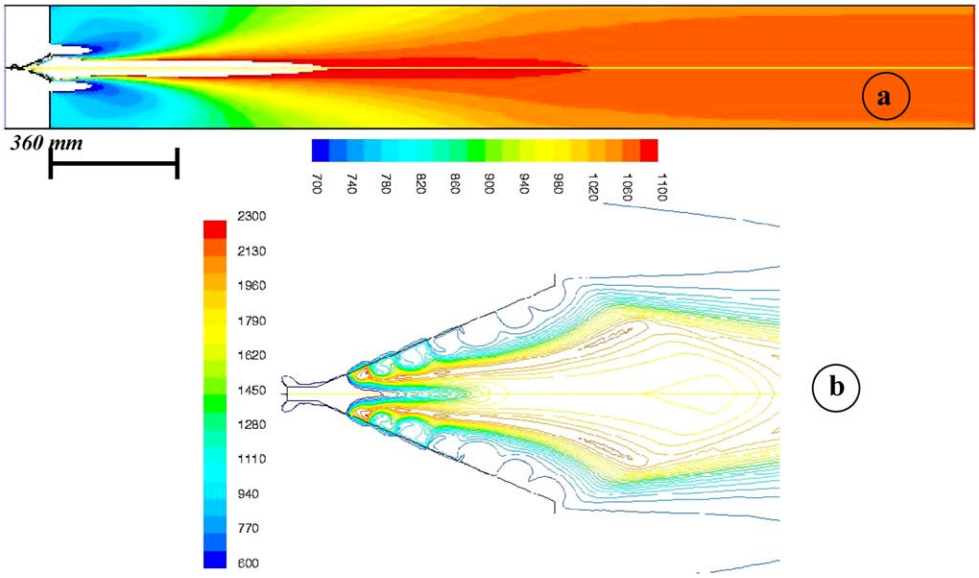

Fig. 9. Distribution of the temperatures (K) inside the combustion chamber (a) and inside the burner (b).

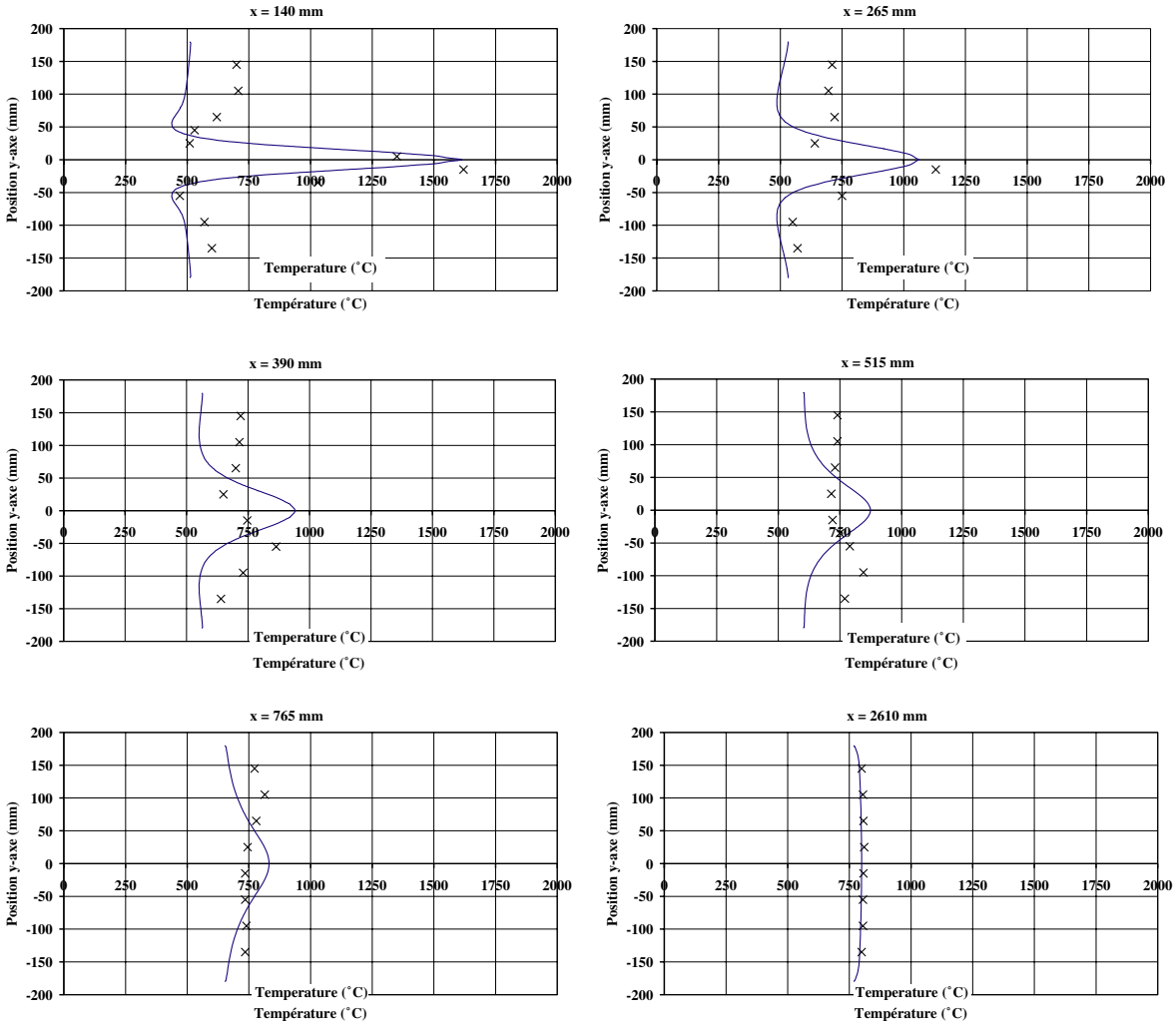

Fig. 10. Comparison of experimental (×) and computed (—) temperature profiles.

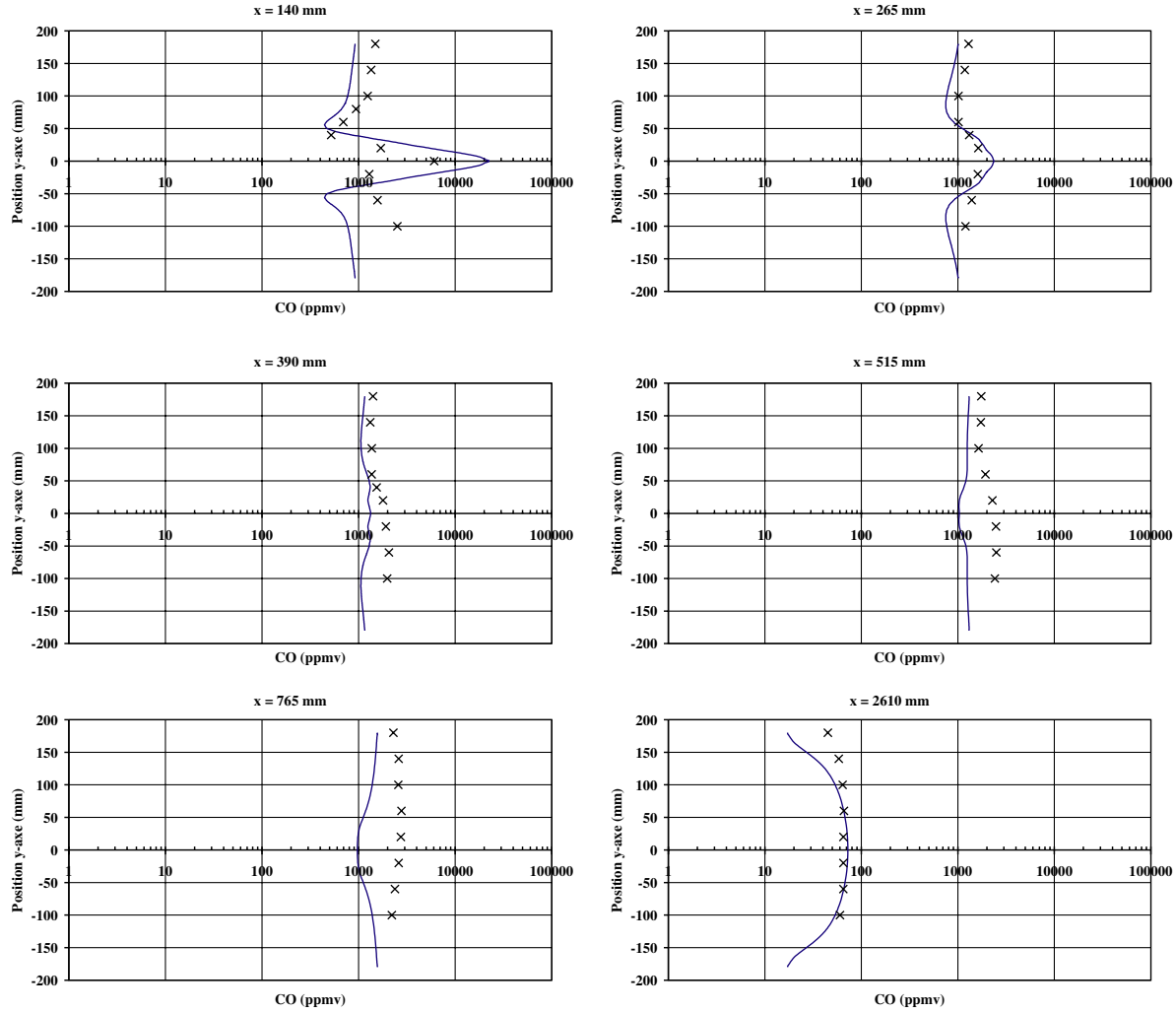

Fig. 11. Comparison of experimental (×) and numerical (—) CO concentration profiles.

radial access at different x along the CC was used for this purpose. The comparison of the computed and experimentally determined CO profiles given in Fig. 11 indicates that acceptable prediction was achieved. It should be recalled here that the pre-exponential factor for the reverse reaction that converts CO_2 into CO was adjusted in the model to fit experimental results at the exit of the CC. The model retrieves a peak in the zone downstream of the burner, followed by a uniform profile after $x = 390$ mm. The model underestimates the CO concentrations in the zone $x = 515$–2610 mm. The bad description of the CO field is probably due to the very simple reaction scheme that was adopted. One can note that the experimentally determined NO concentration fields are not symmetrical.

A simulation was run in which no VOC was present in the air flux; it indicated that no CO was present at the exit of the CC. Consequently, CO results from the combustion of VOCs only; this is a relevant result of this study.

The prediction of NO concentration was computed through kinetic expressions in which no parameter was adjusted. The comparison of the computed and of the experimentally determined profiles given in Fig. 13 shows that NO concentrations are overestimated by 35 ppm in the zone $x > 400$ mm. In the zone close to the burner, the experimentally found peak concentration close to the symmetry plane is retrieved by the model up to $x = 265$ mm.

The model indicates that NO is produced in the flame zone of the burner only; this is in accordance with the results of Stansel et al. [4]. As a consequence, treating an air flow with a high concentration of VOCs will result in a lower power at the burner, and consequently will reduce NO emissions. Again, one can note that the experimentally determined NO concentration fields are not symmetrical.

4.5. CO oxidation into CO_2 limitation

Of particular interest is the examination of Fig. 12, in which we compare the Arrhenius rate and the micro-mixing rate for the destruction of CO using the ratio of the two: W_{CO}. In a zone centred on the symmetry plane, which is thin close to the burner but very large in the left-hand half of the volume of the CC, W_{CO} is larger than 1. This

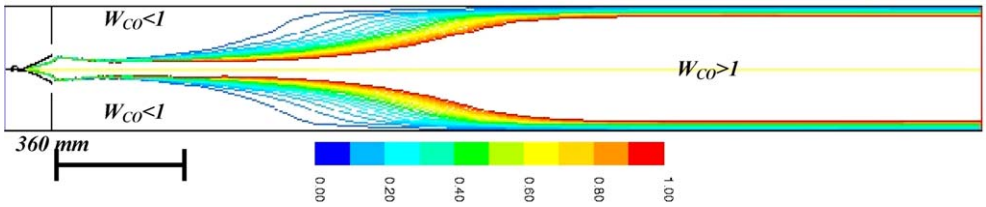

Fig. 12. Distribution of the ratio between the chemical reaction rate and the micro-mixing reaction rate.

indicates that, in this zone, the Arrhenius reaction rate is larger than the micro-mixing reaction rate. The latter is consequently limiting the destruction of CO. The ratio W_{CO} can be lower than 0.2, indicating that the Arrhenius rate can be over 5 times smaller than the micro-mixing rate. In other cases (iso-curves not represented for clarity) the Arrhenius rate is much higher than the micro-mixing rate. This result is of particular interest for industrial application: it indicates that the turbulence intensity should be increased in this zone in order to reduce CO emissions. In a previous experimental work [6], proof was made that adding barrels in this zone did reduce CO emissions significantly.

4.6. Asymmetry of the flow

The temperature, CO concentration and NO concentration experimental measurements performed in the CC indicated a non-symmetrical pattern inside the CC despite the symmetry of its arrangement. Following this intriguing observation, a cold experiment was performed on the pilot unit, and velocity measurements were taken using a hot

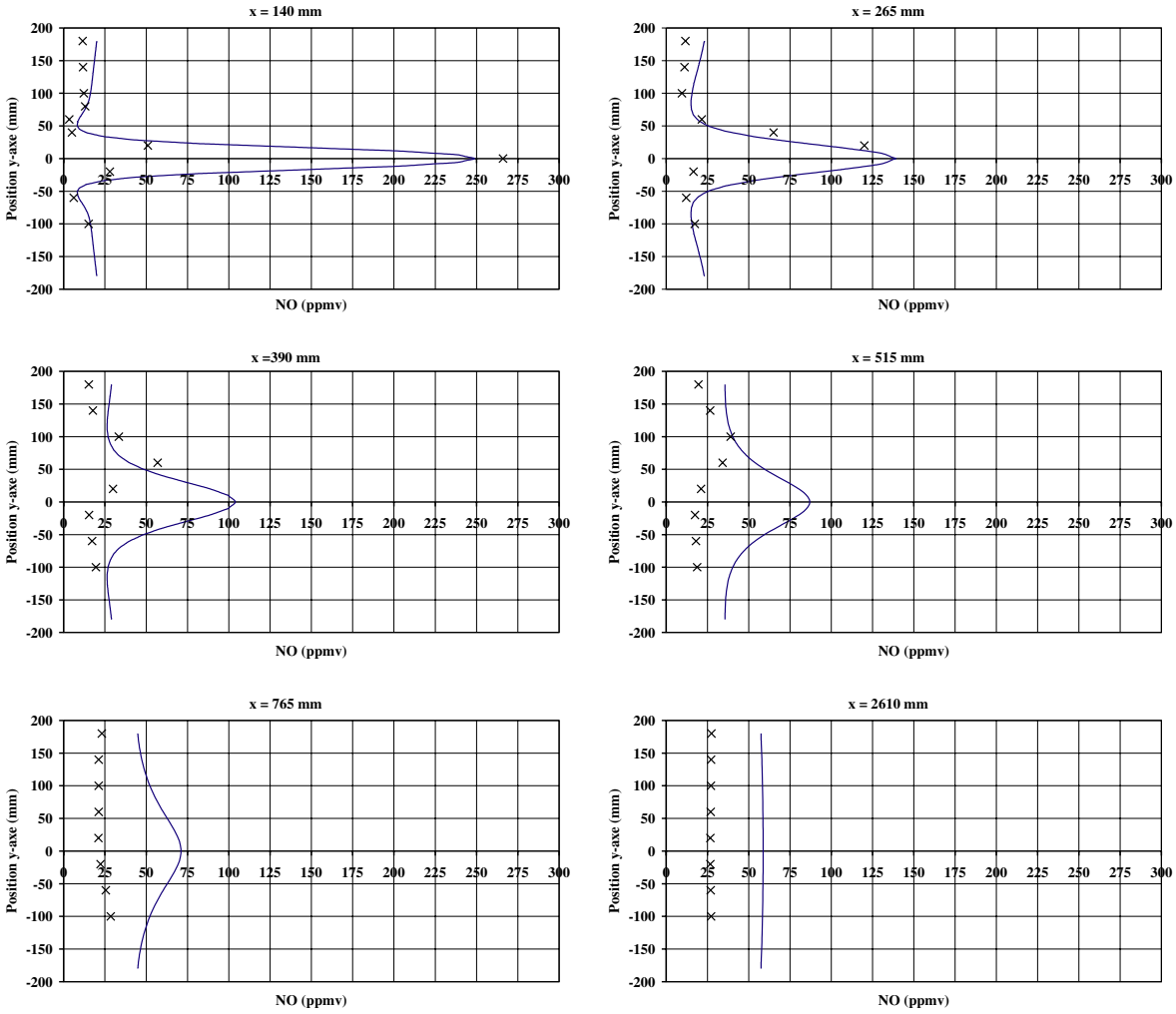

Fig. 13. Comparison between the experimental (×) and numerical (—) NO concentration profiles.

Table 4
Boundary conditions for the cold experiment and hot wire anemometry measurements

Air feed velocity (flow rate of 550 m^3/h STP)	$V_{air} = 1.47$ m s^{-1} (at 20 °C)
Air feed temperature	$T_e = 20$ °C
Height of the air veins	$H_v = 30.5$ mm

wire anemometer (Dantec Streamline 90N10). The 1 μm-diameter wire was placed perpendicular to the x–y plane, and the average total velocity was measured. In parallel, modelling of the complete CC (not only one side of the symmetry plane) was performed using the boundary conditions as indicated in Table 4. The results from the two approaches are reported in Fig. 14. It is clear – from both the experimental approach and from the modelling – that the flow pattern inside the CC is not symmetrical.

The adoption of a 2D description might have caused a computation artefact that did not correspond with reality. Two infinite flat jets parallel to a wall might create a low pressure zone causing the jets to deviate. 3D modelling was then also performed for the TRI; the solution also indicated the deviation of the flow. The 3D modelling indicated that the flow downstream of the burner rapidly lost the structure of the cylindrical jets through the holes of the burner wings and of the NG injection ramp, and turned out very similar to the 2D modelling. We concluded from this that the flow is actually non-symmetrical in the CC despite its symmetrical geometry. Observation of the flame in the pilot unit was easy thanks to numerous optical ports that were installed [3,5]. The deviation of the flame was clearly observable.

5. Conclusion

The use of a commercial CFD code enabled us to model the combined phenomena of fluid flow, heat transfer and chemical reaction progress inside the combustion chamber of a TRI. The predictions of the model are satisfactorily in concordance with experimental measurements.

The design of the actual TRI is globally satisfactory: the flow through the combustion chamber is close to a plug

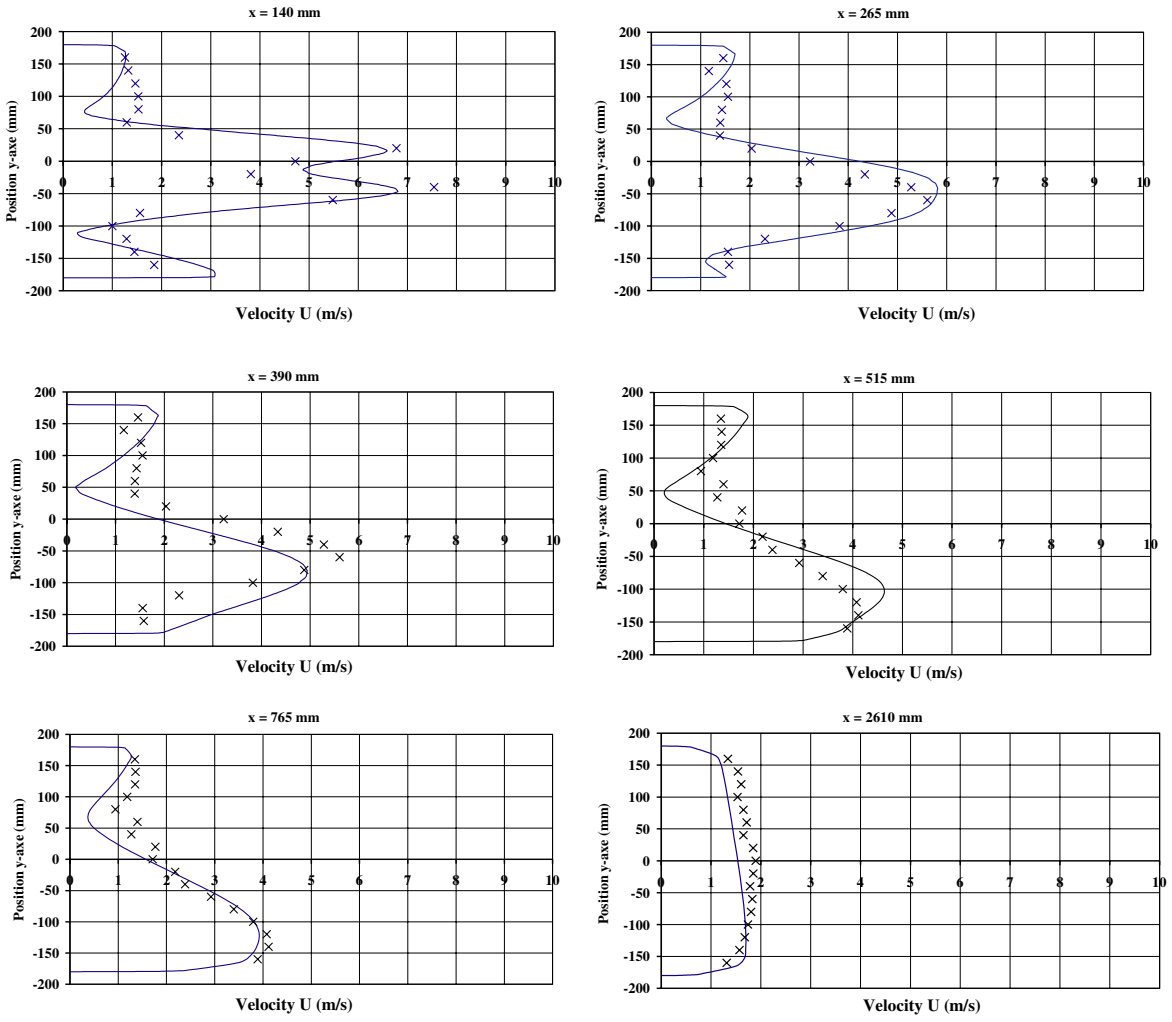

Fig. 14. Comparison between the experimental (×) and computed (—) total average velocity when simulating the whole volume of the chamber (not only one half).

flow both in terms of the velocity field and of the temperature field.

This modelling work reveals – and this is confirmed by experimental measurements – that despite the symmetrical arrangement of the combustion chamber, the flow pattern in a single ramp configuration is not symmetrical. The two air veins deviate from the horizontal plane, affecting both velocity and temperature fields. In the case of H or I-shape arrangement of burner ramps, this deviation is probably less marked.

The destruction of CO is the constraint that keeps the exit temperature at a minimum value. The present work establishes that this CO results from the combustion of the VOC, and not from the combustion of the natural gas. Concentrating VOCs in an air flow prior to the treatment by a TRI will reduce CO_2 emissions, and, since NO is formed only at the burner, will limit NO emissions.

The turbulence intensity is very high until 400 mm downstream of the burner, and quite uniform at a lower value of 200 down to 59% in the rest of the CC. The model indicates that this intensity is not sufficient: micro-mixing is the limiting phenomenon of the reaction of CO oxidation into CO_2. This work indicates the need to increase turbulence intensity using additional devices, to be placed in a clearly identified zone. This was empirically observed in previous experimental work.

The model also retrieves the expected result that NO is formed only in the hot flame zone of the burner; this is compatible with a previous experimental work.

References

[1] M. Akbar, J.A. Barnard, Slow combustion of méthyl éthyl ketone, Trans. Faraday Soc. 64 (1968) 3035–3048.

[2] H. Alteinkirch, G. Stoltengurg, M.H. Wagner, J. Neurol. 219 (1978) 159.

[3] Y. Kara, Oxydation thermique des Composés Organiques Volatils en épurateur récupératif – Optimisation des outils de dimensionnement, Thèse de Doctorat (PhD) de l'INP Toulouse, France, 2003.

[4] D.M. Stansel, N.M. Laurendeau, D.W. Senser, CO and NO_X emissions from controlled-air burner: experimental measurements and exhaust correlations, Combust. Sci. Technol. 104 (4–6) (1995) 207–234.

[5] S. Salvador, Y. Kara, J.-M. Commandré, Reduction of NO emissions of a VOC recuperative incinerator by dilution of the fuel supply, Appl. Therm. Eng. 24 (2004) 245–254.

[6] S. Salvador, Y. Kara, J.-M. Crussol, Improving VOC recuperative incinerators performances by increasing turbulence levels inside the combustion chamber – experimental results, Appl. Therm. Eng. 25 (2005) 1871–1881.

[7] Y. Kara, S. Salvador, J.-M. Commandré, Thermal oxidation of volatile organic compounds in recuperative incinerator – optimisation of the operating parameters and of the geometry, Waste Engineering Congress, Ecole des Mines d'Albi, mai 2005.

[8] Fluent 5 User's Guide, vol. 2, 1998.

[9] F. Marias, J.R. Puiggali, Simulation numérique d'un brûleur industriel. Analyse qualitative des effets de swirl sur l'écoulement et sur la production de polluants, Int. J. Therm. Sci. 39 (2000) 249–264.

[10] D.J. Hautman, F.L. Dryer, K.P. Schug, I. Glassman, A multiple-step overall kinetic mechanism for the oxidation of hydrocarbons, Combust. Sci. Tech. 25 (1981) 219–235.

[11] F.L. Dryer, I. Glassman, High-temperature oxidation of CO and CH_4, 14th International Symposium on Combustion, 1972, pp. 987–1003.

[12] C.K. Westbrook, F.L. Dryer, Simplified reaction mechanisms for the oxidation of hydrocarbon fuels in flames, Combust. Sci. Tech. 27 (1981) 31–42.

[13] D.F. Fletcher, B.S. Haynes, F.C. Christo, S.D. Joseph, A CFD based combustion model of an entrained flow biomass gasifier, Appl. Math. Model. 24 (2000) 165–182.

[14] W. Polifke, K. Döbbeling, T. Sattelmayer, D.G. Nicol, P.C. Malte, A NO_X prediction scheme for lean-premixed gas turbine combustion based on detailed chemical kinetics, J. Eng. Gas Turb. Power 118 (1996) 765–772.

[15] N. Chigier, Energy, Combustion and Environment, McGraw-Hill, 1981.

[16] J. Warnatz, NO_X formation in high temperature processes, VKI Aussois, 1994.

[17] B.F. Magnussen, B.H. Hjertager, On mathematical models of turbulent combustion with special emphasis on soot formation and combustion, 16th International Symposium on Combustion, The Combustion Institute, 1976.